CrossMark

The influence of hierarchical zeolite composition and pore structure on behavior of cobalt-based Fischer–Tropsch synthesis catalysts

Weiming Zhao[1] · Yuelun Wang[1] · Zhuo Li[2] · Hui Wang[2] · Jinhu Wu[2] ·
Jun Huang[1] · Yunpeng Zhao[1]

Abstracts Cobalt catalyst supported on hierarchical zeolite possessing a three different Si/Al ratio was studied in Fischer–Tropsch synthesis. The catalyst with Si/Al ratio of 60 was found to be superior to other catalysts in terms of better C_{5-18} selectivity and higher olefin/paraffin ratio due to smaller cobalt particles and larger number of acidic sites. While Co/Meso-ZSM120 catalyst with perfect crystal structure favored products to accessibility and prevented cobalt particles from being oxidized compared to that of amorphous support, resulting in the lowest deactivation rate and the lowest carbon content on the surface.

Keywords Hierarchical zeolites · Si/Al ratio · Cobalt catalyst · Deactivation · Fischer–Tropsch synthesis

1 Introduction

As one of the most promising routes to solve the energy crisis, converting syngas ($CO + H_2$) to liquid oil by Fischer–Tropsch synthesis (FT synthesis) has attracted more and more attention [1–3]. Co-based catalysts are often the choice for low temperature FT synthesis due to the high stability, high conversion, and high selectivity to linear paraffins, low water–gas shift (WGS) activity, and relatively low price [4, 5]. However, linear paraffins are predominate in FT synthesis, and their distribution follows the Anderson–Schultz–Flory (ASF) law. It is not easy to directly synthesize hydrocarbons with narrow, specified carbon number distribution from FT reaction alone. Furthermore, hydrocracking and isomerization by acidic zeolite are often utilized to convert the heavy FT linear hydrocarbons into liquid fuels.

To directly obtain branched hydrocarbons through FT synthesis without further upgrading of FT products, intensive efforts have been dedicated to modifying cobalt-based catalysts. The catalysts combing with zeolites which were used in isoparaffins synthesis have become a focus of attention over years [6–12]. But in these catalytic systems, the primary hydrocarbon products migrated into micropores of zeolites where the hydrocracking occurs, then the products must diffuse out of the micropores. Such slow transportation of products usually causes over-cracking, resulting in high selectivity of CH_4. The strong acidity of zeolites may also cause the over-cracking of hydrocarbon products. Moreover, these catalysts often suffered very low CO conversion. Their extremely low reduction degree originated from strong interactions of cobalt with zeolites.

Recently, zeolites with hierarchically porous structures have garnered much attention due to their highly attractive properties. Because they combine the catalytic features of micropores and the increased molecular transport within a single body [13–15]. The use of mesoporous zeolites as supports gave promising perspective for FTS [16–18]. Mesoporous H-ZSM-5 zeolites with FTS active phases have demonstrated that the intimate contact between the FTS metal and the acid sites of mesoporous zeolites turned out to be the key parameter, determining the performance of such catalysts in tuning the product selectivity. When acid site domains are in a close vicinity to FTS sites, the

✉ Yuelun Wang
   wangyuelun@126.com

1   Key Laboratory of Coal Processing and Efficient Utilization, Ministry of Education, School of Chemical Engineering, China University of Mining and Technology, Xuzhou 221116, Jiangsu, China

2   Key Laboratory of Biofuel, Chinese Academy of Sciences, Qingdao Institute of Bioenergy and Bioprocess Technology, Qingdao 266101, China

produced olefinic FTS hydrocarbons may crack or iso-merize before they are hydrogenated. Besides, the improved transport properties of hierarchically structured zeolites increase the selectivity toward liquid hydrocarbons. Their high mesopore surface area improves cobalt dispersion at elevated metal loadings. However, limited knowledge is available on the actual role of zeolite acidity and on the influence of the zeolite support on the Co active phase. In this work, a detailed of evaluation of catalyst performance combined with a characterization to understand the bifunctional FTS catalysts with three different Si/Al ratios of 60, 80 and 120 was carried out.

2 Experimental

2.1 Samples preparation

Mesoporous ZSM-5 was prepared as follows: first, 2.409 g of sodium aluminate were dissolved in 30 mL of tetrapropylammonium hydroxide (25 %), together with 65.5 ml of water and 0.191 g of sodium hydroxide, a certain amount of TEOS, prepared with Si/Al molar ratio of 60, 80, 120, respectively, were added to this solution. After homogenization, cetyltrimethylammonium bromide solution (CTAB) was added. The suspension obtained was maintained under mechanical agitation for 2 h. The mixture was heated at 413 K and kept at this temperature for 72 h in hydrothermal vessel. The obtained solid by centrifugation was washed with deionized water and then dried at 333 K for 12 h. The sample was then calcined at 823 K for 5 h. Ion exchange was performed using 1 M solution of NH_4NO_3 at 353 K for 4 h by two consecutive similar processes. After the ion exchange, the zeolite was filtered and washed with enough de-ionized water and after that dried in oven at 363 K overnight, the NH_4-zeolite was calcined in the static air at 773 K for 3 h to obtain meso-H-zeolite. The synthesized materials were named as Meso-ZSM60, Meso-ZSM80 and Meso-ZSM120 corresponding to Si/Al molar ratio of 60, 80, 120, respectively.

The supported cobalt catalysts were prepared by incipient wetness impregnation method. 3 g of different supports were completely wetted with deionized water to evaluate the corresponding volume. Then, cobalt nitrate was dissolved into the required deionized water to impregnate the supports with the loading of 15 %. The catalysts were then dried under temperature of 333 K and calcined at 673 K for 4 h. The obtained catalysts were named Co/Meso-ZSM60 catalyst, Co/Meso-ZSM80 catalyst, Co/Meso-ZSM120 catalyst, respectively. The real cobalt mass content was analyzed by inductively coupled plasma (ICP) technique. A slight change between the design value and the actual value was obtained.

2.2 Characterization

The textural properties of supports and catalysts were determined by nitrogen adsorption and Ar adsorption, in a Micromeritics equipment. The surface area was calculated using the Brunauer–Emmett–Teller (BET) method. The pore size distribution was determined by NLDFT method.

X-ray diffraction (XRD) patterns of the samples were recorded on a Bruker B5005 diffractometer using Cu Ka radiation. The mean Co_3O_4 crystallite sizes were deduced from the XRD data using the Scherrer equation.

TPR was carried out in a U-tube quartz reactor at the ramp rate of 10 K/min in the 5 % H_2/Ar (vol.) flow of 30 ml/min. The H_2 consumption was monitored with TCD using the reduction of CuO as the standard. The reduction percentage of the cobalt oxides was calculated from the TPR profiles.

Temperature-programmed desorption of ammonia was performed with a Chem TPR/TPD instrument (Quantachrome). Approximately 80 mg catalyst was activated for 1 h at 773 K heating with a ramp of 10 K/min. After cooling to 473 K, pure ammonia was passed through the sample. The desorption of the ammonia was accomplished by purging helium with a flow of 20 ml/min and raising the temperature to 1073 K. The effluent gas was analyzed by an on-line gas chromatograph with a TCD detector.

TEM was performed with an FEI Tecnai TF20 microscope using a carbon-coated Cu grid.

2.3 Catalytic experiments

1 g of catalysts were evaluated in a pressured fixed-bed reactor at 2 MPa, 1000 h^{-1} with H_2/CO ratio of 2 after reduction at 673 K for 10 h. Wax was collected with a hot trap and the liquid products were collected in a cold trap. The gas effluents were analyzed on-line by using carbon molecular sieve column with TCD. The gas hydrocarbons were analyzed on-line using Porapack-Q column with FID. Oil and wax were analyzed offline in OV-101 capillary columns. 5 % N_2 was added to syngas as an internal standard. The carbon balance and mass balance were 100 ± 5 %.

3 Results and discussion

The N_2 physisorption isotherms of cobalt supported hierarchical zeolites were presented in Fig. 1. The isotherm of catalysts exhibited the composite isotherms consisted of types II and IV, indicating the existence of micropore and mesopore structures, respectively. Moreover, the shape of the hysteresis loops of supports fell within the H3 category [19], which was attributed to slit-type pores associated with
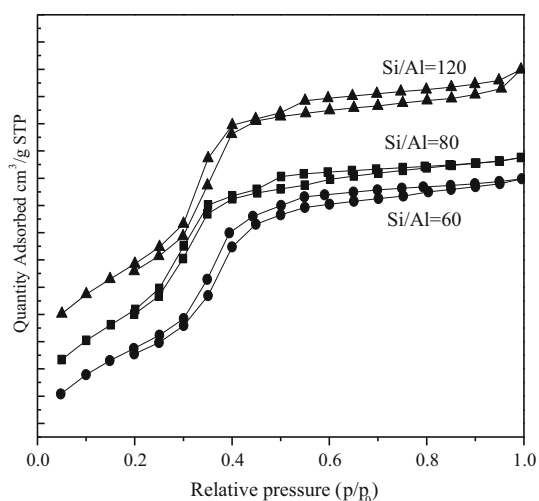
Fig. 1 N$_2$ adsorption/desorption isotherm of catalysts at 70 K

the interparticle porosity generated in solids. The abrupt increase observed in the region of $0.2 < P/P_0 < 0.4$ was a result of micropore filling. The second mild increase within the $0.5 < P/P_0 < 0.9$ region indicated capillary condensation of N$_2$ in mesopores. Figure 2 displayed the pore size distribution of samples. We can note that hierarchical zeolites showed a bimodal distribution with the narrow porosity around 0–2 and 3–5 nm, respectively. The specific surface areas for unloaded supports and loaded supports were reconfirmed by Ar adsorption–desorption analysis. The results of textural properties of supports and catalysts with argon gas are shown in Table 1. It was observed that the change trend of loaded supports was consistent with that of unloaded supports with different Si/Al ratios. An increase on the area of the samples was observed with the increase of Si/Al molar ratio. As a consequence, Co/Meso-ZSM60 catalyst showed the lowest specific surface area and the lowest mesopore volume, while the highest surface
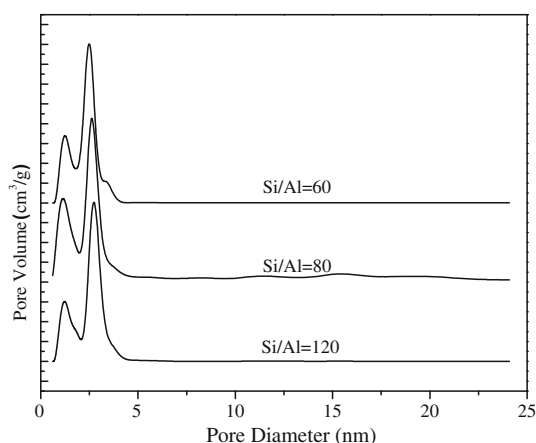
Fig. 2 Pore size distribution of catalysts

area and the largest mesopore volume were found over Co/Meso-ZSM120 catalyst. And its total pore volume increased from 0.91 to 1.01 cm^3/g, which was due to the creation of more mesopores at the cost of a slight decrease in the micropore volume.
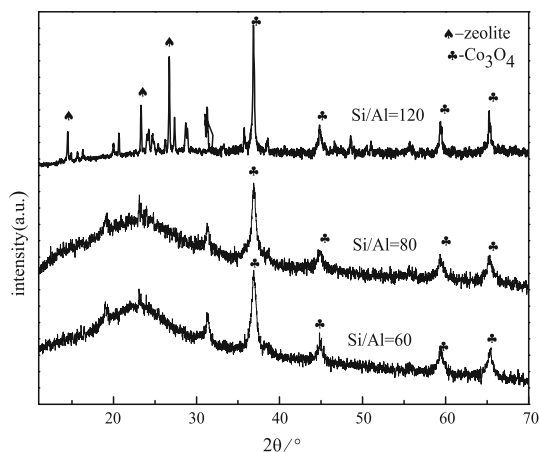
The XRD patterns of Co supported catalysts are presented in Fig. 3. All catalysts showed the characteristic reflection peak at $2\theta = 36.8°, 44.8°, 59.3°,$ and $65.2°$ due to the presence of Co$_3$O$_4$ phase [20, 21]. The particle size of Co$_3$O$_4$ is calculated by using Scherrer's equation. The crystallite size of Co$_3$O$_4$ was found to increase slightly with the increase of Si/Al ratio of hierarchical zeolites, i.e., cobalt particle size of 12.4, 14.2 and 15.8 nm on cobalt catalyst having Si/Al ratios of 60, 80 and 120 as summarized in Table 1. Additionally, the characteristic peaks of MFI structure were observed on Co/Meso-ZSM120 catalyst. There was a diminution of XRD peaks intensities with decreasing Si/Al molar ratio, i.e., Co/Meso-ZSM60 catalyst, presented a strong diminution of the zeolite XRD peaks intensity, suggesting the amorphism structures were present.

Figure 4 displays the TPR profiles of catalysts, where one observed three peaks corresponding to the transitions of Co$_3$O$_4$. The first peak was assigned to the reduction of the Co^{3+} phase to Co^{2+} at about 598 K for the catalysts with Si/Al ratio of 80 and 120, while Co/Meso-ZSM60 catalyst showed this reduction peak at about 623 K due to smaller particles of cobalt oxide. The second peak occurred at a higher temperature corresponding to the transition Co$^{2+} \rightarrow$ Co^0. With the increase of Co$_3$O$_4$ particle sizes, the positions of the peaks shifted to lower temperatures, which suggested that larger particles were more facilitated the rate of Co reduction. However, the third peak overlapped and extended over a wide temperature range, indicating several interactions occurring between the cobalt species and the surface of supports, which led to the formation of unreductive cobalt aluminates or cobalt silicates. With the decrease of Si/Al ratios, the areas of reduction peak were increased indicated that the cobalt-support interaction became more complicated and stronger [22, 23]. The reduction degree was relatively expressed as the ratio of the amount of H$_2$ consumption below 673 K to that of total H$_2$ consumption. The values were 69.3, 73.2, 78.4 % for the catalysts with Si/Al ratio of 60, 80, 120, respectively, as shown in Table 1.

The morphology of coalt supported mesoporous ZSM-5 was verified using TEM. For Co/Meso-ZSM120 catalyst, the small zeolitic MFI particles (Fig. 5a) lied at the edges of the mesoporous phase which was partly worm-like (Fig. 5b). For Co/Meso-ZSM60 catalyst, amorphous structure was observed. These demonstrated that the material with zeolitic features with retaining a narrow mesoporous distribution was a composite and not a true

Table 1 Texture and phase structure properties of supports and cobalt catalysts

Samples	Specific surface area (m^2/g)	Micropore size (nm)	Mesopore size (nm)	V_{micro} (cm^3/g)	V_{meso} (cm^3/g)	Average Co$_3$O$_4$ particlesize (nm)	Reducibility (100 %)	Total acid sites (mmoles NH$_3$/g)
MZ60	976	1.8	4.5	0.67	0.32			
MZ80	1098	1.3	4.3	0.62	0.38			
MZ120	1198	1.6	4.7	0.60	0.53			
Co/MZ60	792	1.8	4.0	0.63	0.28	12.4	69.3	0.67
Co/MZ80	912	1.2	4.2	0.58	0.35	14.2	73.2	0.56
Co/MZ120	1014	1.5	4.5	0.56	0.45	15.8	78.4	0.37

Fig. 3 XRD profiles of the prepared catalysts
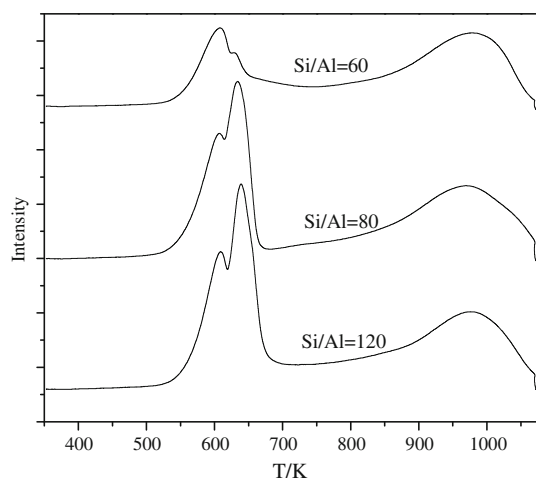
**Fig. 4** TPR profiles of the prepared catalysts

interconnected hierarchical mesoporous zeolite. The presence of separate mesoporous and zeolitic phases was due to the underlying competition in interaction between zeolite and mesopore formation [24]. TEM images also showed that Co oxide crystallites of about 10–50 nm were located in the interconnected pores of meso-ZSM-5 particles.

Further, some Co crystallites were visibly tended to cluster on the support.

The NH$_3$-TPD patterns of the FT catalysts are shown in Fig. 6 and two NH$_3$ desorption peaks were observed. The lower-temperature peak centered at 453–523 K could be assigned to ammonia desorption over the weak acid sites [18]. It was observed that the intensity of weak acid sites was higher on Co/Meso-ZSM60 catalyst, in the first desorption temperature region, which was ascribed to be the presence of a higher amount of Al species in Co/Meso-ZSM60 catalyst [25]. A broad peak at 573–993 K, which could be attributed to the adsorption of acid sites, was observed. The peak at approximately 723 K was ascribed to the strong acid sites. Table 1 gives the number of acid sites expressed as mmol NH$_3$/g of catalyst with respect to only weak and strong acidic sites. By considering first peak only (weak acid sites), the total number of acid sites varied in the order of Si/Al = 60, 80, 120. As a coincidence, the acidity decreased proportionately with the increase in Si/Al ratio of the support. Besides, the intensity of desorption peak at 723 K decreased remarkably when Si/Al ratio increased, which was easy to understand that there was less acidity of strong acid sites at lower aluminum concentration. The cobalt particle size may have an influence on the surface acidity. A weaker interaction was present between larger cobalt particles and the support with lower surface acid sites.

The catalytic performance on cobalt catalysts was measured at 503 K. The activity of Co/Meso-ZSM120 catalyst was the highest among the catalysts. That is, CO conversion proportionately increased with the increase of Si/Al ratio and this trend also correlated with cobalt particle sizes in larger mesopores as shown in Table 1. These larger particle sizes were responsible for higher reducibility of catalysts, which was found to be preferable for better CO conversion. Co/Meso-ZSM60 catalyst showed the lowest activity due to strong acidity of the support and the high dispersion of cobalt particles which resulted in less active sites for the chemisorption of CO, and thus in a decrease of activity.
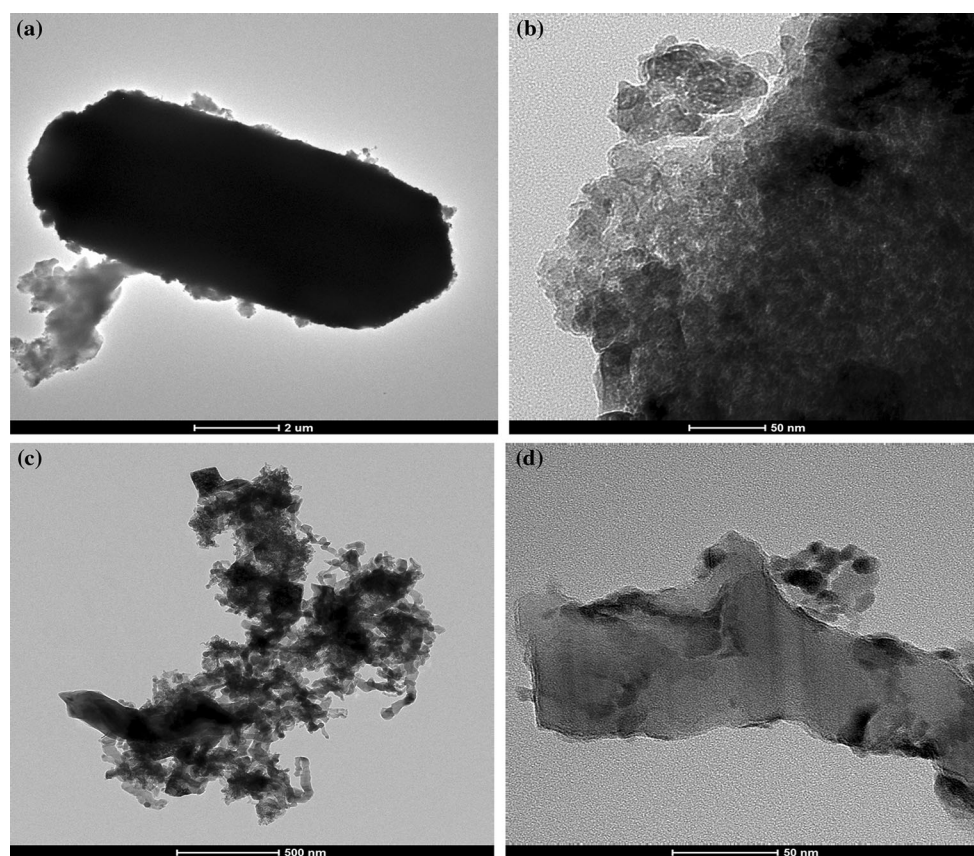
Fig. 5 TEM of Co/Meso-ZSM120 (**a**), Co/Meso-ZSM120 (**b**), Co/Meso-ZSM60 (**c**) Co/Meso-ZSM60 (**d**)
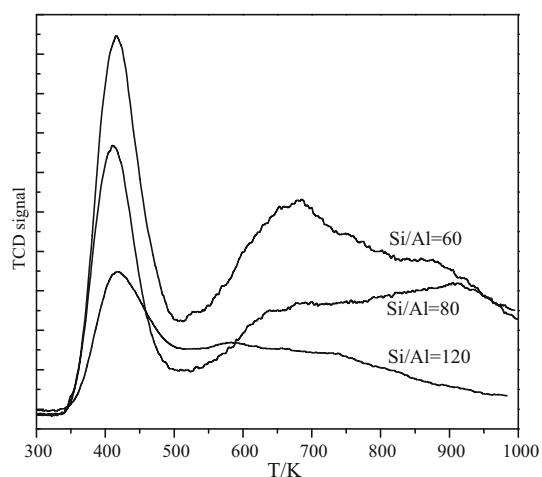
Fig. 6 NH$_3$-TPD profiles of catalysts

The selectivities of the FTS catalysts were significantly depending on their pore structure as showed in Table 2. The catalyst having smaller pore sizes tended to produce lighter hydrocarbons. As the pore size was larger, primary products transported more effectively and relevantly methane formation rate from secondary hydrocracking of

olefins was lower. Accordingly the proportion of the heavy hydrocarbon was higher. In this study, zeolites with hierarchically porous structures combined the catalytic features of micropores and the increased molecular transport within a single body. The formation of the hierarchical composite catalysts with both zeolite and mesoporous materials gave rise to the increase of middle distillates because large space of the mesoporous material in zeolite promoted the generation of the more bulky branched hydrocarbons and decreased the selectivity of methane in FT synthesis. Co/Meso-ZSM120 catalyst showed the highest selectivity towards C$_{18+}$ hydrocarbon products due to the presence of larger mesopores with the increased transport properties of FT products and larger cobalt particles resulting in higher reducibility.

A lower olefin/paraffin (O/P) was also observed due to higher activity of hydrogenation and the suppressed olefin cracking properties of heavy olefinic products over lower acid sites [26]. Since the presence of strong acid sites on zeolite was responsible for the formation of isomers and aromatics [27], the ratio of isoparaffins to n-paraffins in the range of C$_{5-18}$ (denoted as C$_{iso}$/C$_n$), an indicator of the quality of middle distillates, also increased with the increase of acid sites due to the secondary reactions,

**Table 2** Catalytic performance of cobalt catalysts in FT synthesis

Catalyst	CO conversion (%)	C_1 (%)	C_{2-4} (%)	C_{5-18} (%)	C_{18+} (%)	O/P[a]	C_{iso}/C_n [b]	Deactivation rate[c]
Co/Meso-ZSM60	42.3	20.5	9.6	61.7	8.2	0.68	0.81	0.78
Co/Meso-ZSM80	56.2	19.4	9.4	60.7	10.5	0.57	0.70	0.64
Co/Meso-ZSM120	67.5	19.2	8.6	59.6	12.6	0.48	0.52	0.19

Reaction conditions: H_2/CO = 2, GHSV = 1000 h^{-1}, P = 2 MPa, T = 503 K, TOS = 24 h

[a] O/P stands for the olefin-to-paraffin ratio in the range of C_1–C_{30} hydrocarbons

[b] C_{iso}/C_n stands for isoparaffin to n-paraffin in the range C_5–C_{18}

[c] deactivation rate: (CO conv. at 24 h—CO conv. at 312 h)/(CO conv. at 24 h) × 100
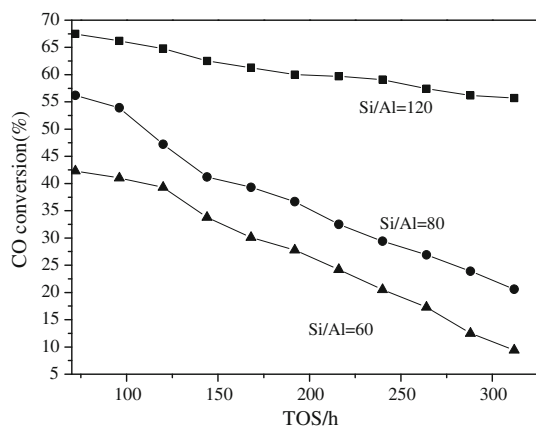

Fig. 7 TOS evolution of CO conversion during FTS at 503 K

including hydrocracking and isomerization of the primary hydrocarbons over the acid sites. The high amounts of acidic sites on the catalyst having a low Si/Al ratio were responsible for obtaining a high selectivity to olefins and C_{5-18} hydrocarbons. Meanwhile, a higher methane selectivity was observed over Co/Meso-ZSM60 catalyst, which was ascribed that lower reducibility of the catalyst led to lower probability of carbon-chain propagation and higher acid sites facilitated hydrocracking reactions.

A gradual deactivation of the catalysts with time-on-stream was observed in Fig. 7. The deactivation rate was calculated and compared to the stability of catalysts in Table 2. It was observed that Co/Meso-ZSM60 catalyst and Co/Meso-ZSM80 showed similar deactivation rate. The fastest rate of deactivation was observed over Co/Meso-ZSM80 catalyst, even though it possessed more acid sites than that of Co/Meso-ZSM120 catalyst. The reason might be related to the different structure of the supports. XRD results showed that Co/Meso-ZSM120 catalyst had perfect crystal structure of ZSM-5, which could prevent particles from being oxidized by water and stabilize cobalt active sites compared to that of amorphous support. It was suggested that water produced increased the oxidation–

reduction cycles on the catalyst surfaces, therefore leading to the growth and sintering of active metallic sites [25]. Moreover, the largest pore volume was found over Co/Meso-ZSM120 catalyst, the products including water removed easier, preventing from the rapid buildup of inactivating species. Thus, the catalyst showed the highest stability among the catalysts.

The crystallinity of mesoporous ZSM5 to the possible cobalt reoxidation was verified by measuring the oxidation states of cobalt particles on the used catalysts through XPS analysis (Fig. 8). The binding energies, as well as the percentage of each species, are summarized in Table 3, the three phases Co_3O_4, CoO and metallic cobalt are represented. For all samples the doublet separation of the binding energy (ΔE) between the Co 2p$^{1/2}$ and Co 2p$^{3/2}$ peaks was 14.8–15.4 eV, which was close to that of the mixed-valence Co_3O_4 (15.2 eV) [28]. Therefore, Co_3O_4 was considered the predominant cobalt phase in used catalysts. The reason might be that metal cobalt was oxidized during the FT reaction then exposed atmosphere after being taken out of reactors. It was noted that the catalysts exhibited a remarkably higher ratio of oxidic Co^{2+} to oxidic Co^{3+} than Co_3O_4. This indicated that some cobalt species existed in the state of CoO or a possibility that cobalt interacted either with Al or Si oxides. The peak intensity of Co2p$^{3/2}$ became enhanced with decreasing Si/Al ratios, indicating the increased content of Co_3O_4 on the catalyst surfaces. The surface atomic ratio of $Co^0/(Co^{2+} + Co^{3+})$ was also presented in Table 3. The highest $Co^0/(Co^{2+} + Co^{3+})$ ratio was observed over Co/Meso-ZSM120 which showed higher reducibility and relative stability in FT synthesis. The wax deposition to catalyst deactivation in the mesoporous ZSM5 was also confirmed by XPS methods to quantify the amount of waxes or cokes on the surface of catalysts (Fig. 9). It can be noticed that the peak intensity of C1 s increased with decreasing Si/Al ratios, indicating the increased content of waxes or cokes on the catalyst surfaces. The lowest carbon content was showed over Co/Meso-ZSM120 catalyst.
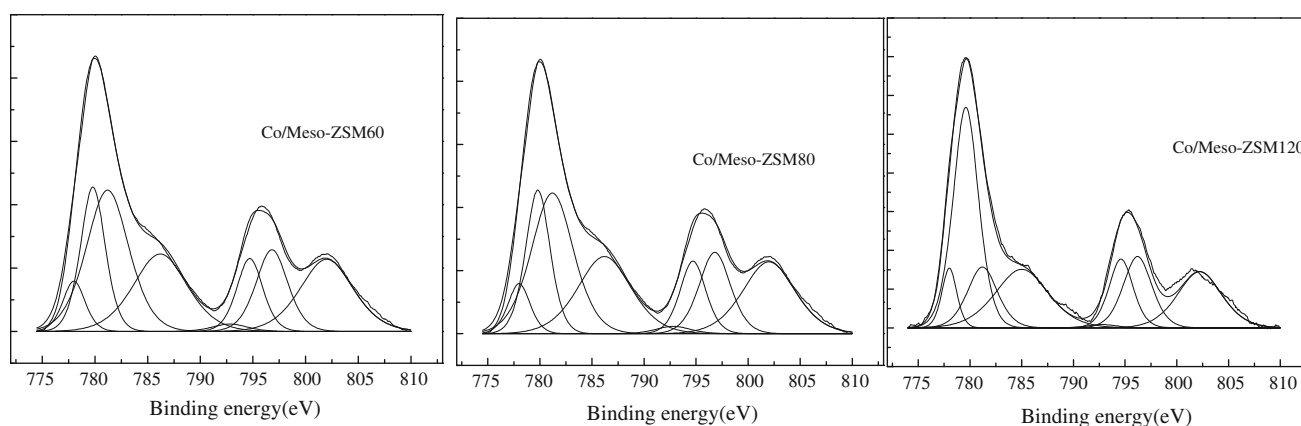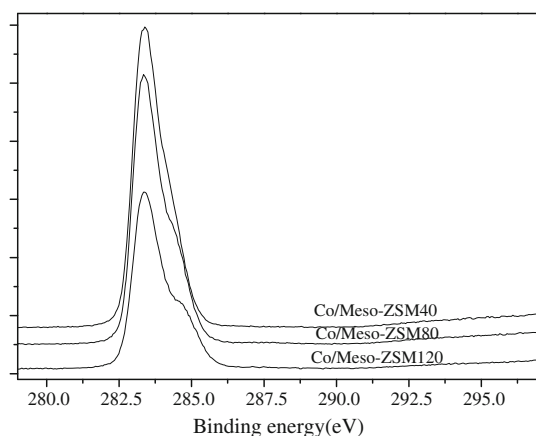
Fig. 8 XPS profiles of the used catalysts

Table 3 XPS results of cobalt catalysts

Sample	Binding energy[a] Co2$_{p3/2}$ (eV)				Binding energy[a] Co2$_{p1/2}$ (eV)				Co^0/Co^{II} + Co^{III}
	Co^0	Co^{III}	Co^{II}	Co^{II} satellite	Co^0	Co^{III}	Co^{II}	Co^{II} satellite	
Co/Meso-ZSM60	778.06 (407.6)	779.53 (891.7)	781.32 (1648.5)	785.09 (1131.4)	792.8 (101.5)	794.77 (742.3)	796.46 (915.1)	802.64 (1093.5)	0.082
Co/Meso-ZSM80	778.06 (164.7)	779.63 (580.5)	781.20 (327.4)	785.09 (403.8)	782.8 (35.936)	794.67 (279.3)	796.24 (232.6)	802.23 (303.1)	0.092
Co/Meso-ZSM120	778.06 (173.5)	779.53 (420.2)	781.21 (418.1)	786.47 (302.4)	792.8 (90.35)	794.77 (179.4)	796.87 (308.8)	802.13 (297.3)	0.137

[a] The values in brackets denote the XPS peak area

Fig. 9 XPS profiles of C1s over the prepared catalysts

was attributed to smaller cobalt particles and larger number of weak acidic sites. For Co/Meso-ZSM120 catalyst, the reducibility of cobalt particles was higher and the concentration of weak acid sites was lower, consequently increasing CO conversion and C_{18}^+ selectivity. The catalyst with perfect crystal structure of ZSM-5 favored products including water to accessibility and prevented cobalt particles from being oxidized compared to that of amorphous support, which was resulted in the lowest deactivation rate and the lowest carbon content on the surface.

4 Conclusion

The effect of Si/Al ratios on hierarchal ZSM-5 for cobalt-based catalyst in FT reaction has been studied in this work. Co/Meso-ZSM60 catalyst showed higher selectivity to C_{5-18} hydrocarbons and higher olefin/paraffin ratio, which

References

1. W. Wang, Y. Chen, Appl. Catal. **77**, 21–36 (1991)
2. E. Iglesia, S.L. Soled, R.A. Fiato, J. Catal. **137**, 212–214 (1992)
3. E. Iglesia, Appl. Catal. A **161**, 59–78 (1997)
4. G. Jacobs, T.K. Das, Y. Zhang, J. Li, G. Racoillet, B.H. Davis, Appl. Catal. A Gen. **233**, 263–281 (2003)

5. A.R. de la Osa, A. de Lucas, L. Sanchez-Silva, J. Diaz-Maroto, J.L. Valverde, P. Sanchez, Fuel **95**, 587–598 (2012)

6. X. Li, K. Asami, M. Luo, K. Michiki, N. Tsubaki, K. Fujimoto, Catal. Today **84**, 59–65 (2003)

7. A. Martınez, C. Lopez, Appl Catal A Gen **294**, 251–259 (2005)

8. Y.W. Chen, H.T. Tang, J.G. Goodwin Jr, J. Catal. **83**, 415–427 (1983)

9. H.H. Nijs, P.A. Jacobs, J. Catal. **66**, 401–411 (1980)

10. P.A. Jacobs, in *Catalysis by Zeolites*, ed. by B. Imelik, C. Naccache, J.C. Vedrine (Elsevier, Amsterdam, 1980), pp. 293–297

11. G.H. Yang, J.J. He, Y. Yoneyama, Y.S. Tan, Y.Z. Han, N. Tsubaki, Appl. Catal. A Gen. **329**, 99–105 (2007)

12. S. Kang, J. Ryu, J. Kim, I. Jang, A.R. Kim, G. Han, J. Bae, K. Ha, Energy Fuels **26**, 6061–6069 (2012)

13. M. Hartmann, Angew. Chem. Int. Ed. **43**, 5880–5882 (2014)

14. J. Perez-Ramırez, C.H. Christensen, K. Egeblad, C.H. Christensenand, J.C. Groen, Chem. Soc. Rev. **37**, 2530–2542 (2008)

15. S.A. Lopez-Orozco, A. Inayat, A. Schwab, T. Selvam, W. Schwieger, Adv. Mater. **23**, 2602–2615 (2011)

16. A.L.C. Pereira, J.M. González-Carballo, F.J. Pérez-Alonso, S. Rojas, J.L.G. Fierro, M.D.C Rangel, Top. Catal. **54**, 179–189 (2011)

17. S. Sartipi, K. Parashar, M.J. Valero-Romero, V.P. Santos, B. Linden, M. Makkee, F. Kapteijn, J. Gascon, J. Catal. **305**, 179–190 (2013)

18. J. Kang, K. Cheng, L. Zhang, Q. Zhang, J. Ding, W. Hua, Y. Lou, Q. Zhai, Y. Wang, Angew. Chem. **123**, 5306–5309 (2011)

19. T. Witoon, M. Chareonpanich, J. Limtrakul, J. Sol–Gel. Sci. Technol. **51**, 146–152 (2009)

20. Manoj Pudukudy, Zahira Yaakob, Superlattices Microstruct. **64**, 15–26 (2013)

21. Masrinda Tasirin, Chem. Pap. **68**, 1087–1096 (2014)

22. Manoj Pudukudy, Zahira Yaakob, Eng. J. **262**, 1009–1021 (2015)

23. M. Pudukudy, Z. Yaakob, Z.S. Akmal, Appl. Surf. Sci. **330**, 418–430 (2015)

24. J. Vernimmen, V. Meynen, S.J.F. Herregods, P. Cool, Eur. J. Inorg. Chem. **27**, 4234–4240 (2011)

25. Agustın Martınez, Carlos Lopez, Appl. Catal. A Gen. **294**, 251–259 (2005)

26. A. Tavasoli, R.M. Malek Abbaslou, A.K. Dalai, Appl. Catal. A **346**, 58–64 (2008)

27. Y.J. Lee, J.Y. Park, K.W. Jun, J.W. Bae, Viswanadham N. Catal. Lett. **126**, 149–154 (2008)

28. J.Y. Luo, M. Meng, X. Li, X.G. Li, Y.Q. Zha, T.D. Hu, Y.N. Xie, J. Zhang, J. Catal. **254**, 310–324 (2008)